NREL
NATIONAL RENEWABLE ENERGY LABORATORY

State-Space Realization of the Wave-Radiation Force within FAST

Preprint

Tiago Duarte and Antonio Sarmento
Technical University of Lisbon

Marco Alves
Wave Energy Centre

Jason Jonkman
National Renewable Energy Laboratory

Presented at the ASME 2013 32nd International Conference on Ocean, Offshore and Arctic Engineering
Nantes, France
June 9-14, 2013

NREL is a national laboratory of the U.S. Department of Energy
Office of Energy Efficiency & Renewable Energy
Operated by the Alliance for Sustainable Energy, LLC.

This report is available at no cost from the National Renewable Energy Laboratory (NREL) at www.nrel.gov/publications.

Conference Paper
NREL/CP-5000-58099
June 2013

Contract No. DE-AC36-08GO28308

This report is available at no cost from the National Renewable Energy Laboratory (NREL) at www.nrel.gov/publications.

Available electronically at http://www.osti.gov/bridge

Available for a processing fee to U.S. Department of Energy and its contractors, in paper, from:

U.S. Department of Energy
Office of Scientific and Technical Information
P.O. Box 62
Oak Ridge, TN 37831-0062
phone: 865.576.8401
fax: 865.576.5728
email: mailto:reports@adonis.osti.gov

Available for sale to the public, in paper, from:

U.S. Department of Commerce
National Technical Information Service
5285 Port Royal Road
Springfield, VA 22161
phone: 800.553.6847
fax: 703.605.6900
email: orders@ntis.fedworld.gov
online ordering: http://www.ntis.gov/help/ordermethods.aspx

Cover Photos: (left to right) photo by Pat Corkery, NREL 16416, photo from SunEdison, NREL 17423, photo by Pat Corkery, NREL 16560, photo by Dennis Schroeder, NREL 17613, photo by Dean Armstrong, NREL 17436, photo by Pat Corkery, NREL 17721.

Printed on paper containing at least 50% wastepaper, including 10% post consumer waste.

STATE-SPACE REALIZATION OF THE WAVE-RADIATION FORCE WITHIN FAST

Tiago Duarte*
Instituto Superior Técnico
Technical University of Lisbon
Lisboa, Portugal

Marco Alves
Wave Energy Centre
Lisboa, Portugal

Jason Jonkman
National Renewable Energy Laboratory (NREL)
Golden, Colorado, USA

António Sarmento
Instituto Superior Técnico
Technical University of Lisbon
Lisboa, Portugal

ABSTRACT
Several methods have been proposed in the literature to find a state-space model for the wave-radiation forces. In this paper, we compared four methods, two in the frequency domain and two in the time domain. The frequency-response function and the impulse response of the resulting state-space models were compared against those derived from the numerical code WAMIT.
A new state-space module was implemented within FAST, an offshore wind turbine computer-aided engineering tool, and we compared the results against the previously implemented numerical convolution method. The results agreed between the two methods, with a significant reduction in required computational time when using the new state-space module.
Keywords: Wave radiation, time-convolution, state-space model, linear potential-flow theory.

NOMENCLATURE
A_r, B_r, C_r	Matrices of the state-space system
R^2	Mean square error
x_r	Radiation states
$A(\omega)$	Frequency-dependent added mass
$B(\omega)$	Frequency-dependent radiation damping
$K(\omega)$	Frequency-dependent retardation function
$K(t)$	Impulse-response function
q	Displacement vector

*Corresponding Author: tduarte@hidro1.ist.utl.pt

1. INTRODUCTION
Floating offshore wind turbines represent a promising way to explore the vast deep-water wind resource available, and a potential ability to supply much of the world's energy needs. To analyze the multiphysical environment that the floating wind systems are subjected to, coupled aero-hydro-servo-elastic tools have been developed and verified in recent years.
FAST [1], developed by the National Renewable Energy Laboratory (NREL), is one of the first coupled tools that was developed for modeling floating offshore wind turbines. HydroDyn, the hydrodynamic module included in FAST, is currently based on linear time-domain potential-flow theory, using the Morison equation to account for viscous-drag contributions. The module employs the general form of the *Cummins* equation, including the effect of hydrostatics, wave excitation, and wave radiation.
In the *Cummins* equation, the free-surface memory effects caused by radiated waves are implemented with a convolution term of the retardation function. This paper focuses on replacing the numerical convolution method by a parametric model, using a linear state-space formulation. This new *SS_Radiation* module will be available in a future FAST release, and it reads externally derived state-space matrices and solves the state-space system for each time step. To derive the matrices, a preprocessor called *SS_Fitting* was implemented in MatLab [2], and is presented in this paper (Figure 1).
This new approach will enable both a loose and tight coupling of the hydrodynamic forces within the new FAST modularization framework. In particular, the tight coupling scheme has the capability to provide better numerical accuracy

and stability of the model than the loose coupling scheme. In addition, it can enable the linearization of the complete aero-hydro-servo-elastic solution, including the wave-radiation forces, which is useful for eigenanalysis and the development of new control algorithms for floating wind systems. Linearization of the convolution method is only possible if the convolution is implemented numerically in discrete time, but then the resulting linearized system must include a combination of continuous and discrete time states. See [3] for more information.

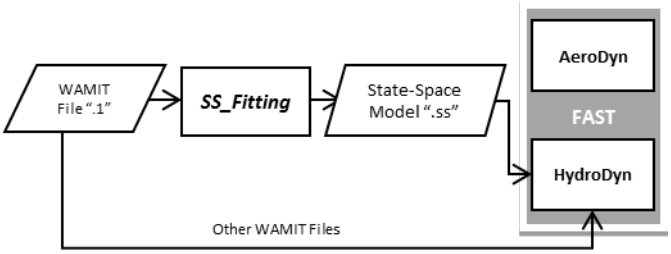

FIGURE 1. MATLAB PREPROCESSOR AND REQUIRED FILES.

2. LINEAR HYDRODYNAMICS

The hydrodynamic forces applied to a floating body can be described by the application of the second *Newton's Law*, for each degree of freedom (DOF):

$$M\ddot{q} = F^{hydrostatic} + F^{radiation} + F^{Waves} \quad (1)$$

Where M is the mass matrix of the floating body, q is the displacement vector, and F is the different hydrodynamic forces acting on the body. These forces include the hydrostatic restitution forces, $F^{hydrostatic}$; added mass and damping from the radiation problem, including free-surface memory effects, $F^{radiation}$; and diffraction forces from incoming waves, F^{Waves}.

2.1. *Cummins* Equation

Under the assumption of linear theory, ideal fluid, and small waves and body motion, Eq. (1) becomes the commonly named *Cummins equation* [4], which can be expressed as:

$$(m + A_\infty)\ddot{q} + \int_0^t K(t-\tau)\dot{q}(\tau)\delta\tau + C^{hydrostatic}q = F^{waves} \quad (2)$$

The term $\left(C^{hydrostatic}q\right)$ represents the hydrostatic force. HydroDyn actually uses a slightly augmented version of Eq. (2), including the impacts of drag forces caused by viscous effects and the mooring line forces.

The coefficients A_∞, K, and $C^{hydrostatic}$ must be computed by a hydrodynamic panel code, such as WAMIT [5], to provide the frequency-dependent added mass and damping matrices, as well as the hydrostatic matrix and frequency-dependent wave-excitation forces.

2.2. Radiation Force

The radiation force arises from the change in momentum of the fluid caused by the motion of the structure. Using the linear wave approximation, the radiation force in an ideal fluid can be represented by the following equation:

$$F^{radiation} = -A_\infty\ddot{q} - \int_0^t K(t-\tau)\dot{q}(\tau)\delta\tau \quad (3)$$

The term $-A_\infty\ddot{q}$ represents the contribution to the force in phase with the acceleration of the device, in which A_∞ is the constant positive infinite-frequency added mass matrix.

The term $-\int_0^t K(t-\tau)\dot{q}(\tau)\delta\tau$ represents the fluid memory effects and incorporates the energy of the radiated waves generated by the motion of the body. This term is represented by the time convolution of the body velocities and the radiation impulse-response function, $K(t)$, also called the *retardation* or *memory* matrix. This is not an easy term to compute numerically, as it requires information from previous time steps (in theory, from the start of the body motion). Most of the codes using this formulation truncate the integral in Eq. (3):

$$F^{radiation} = -A_\infty\ddot{q} - \int_{t-t_{memory}}^t K(t-\tau)\dot{q}(\tau)\delta\tau \quad (4)$$

As a result, only a few seconds (s) of 'memory' (t_{memory}) are stored, usually 60 s. The accuracy of this method depends on the amount of time stored—which increases the computational time—and the impulse-response function of the platform modeled (see Section 5 for more information).

2.3. Relationship Between Time and Frequency Domain

In the frequency domain, the convolution integral of the radiation force becomes the multiplication of the *Fourier* transform of the retardation matrix $K(t)$ by the body velocity $\dot{q}$. The retardation function $K(\omega)$ may be broken down into the following real and imaginary parts:

$$K(\omega) = B(\omega) + j\omega[A(\omega) - A_\infty] \quad (5)$$

The coefficients $A(\omega)$ and A_∞ represent the frequency-dependent added mass and the infinite-frequency added mass, respectively. The term $B(\omega)$ represents the frequency-dependent damping matrix and $j = \sqrt{-1}$. As shown earlier, all of these coefficients may be obtained from a hydrodynamic panel code.

The relation between these matrices and the impulse-response function was derived by Ogilvie [6] by using a direct application of the *Fourier* transform under a sinusoidal regime:

$$A(\omega) = A_\infty - \frac{1}{\omega}\int_0^\infty K(t)\sin(\omega t)\,dt \quad (6)$$

$$B(\omega) = \int_0^\infty K(t)\cos(\omega t)\,dt \tag{7}$$

Where it follows that $A_\infty = \lim_{\omega\to\infty} A(\omega)$. Given the frequency-dependent damping matrix, it is possible to compute the impulse-response function using:

$$K(t) = {}^2/_\pi \int_0^\infty B(\omega)\cos(\omega t)\,d\omega \tag{8}$$

The impulse-response function can be obtained by either using (8) or the inverse Fourier transform of Eq. (5).

3. PARAMETRIC MODELS

To compute the free-surface memory effects more efficiently, it is possible to fit a parametric model to approximate the convolution term in the *Cummins* equation. This can be accomplished (assuming the system is causal and time invariant) by using a state-space model described as:

$$\mu = \int_0^t K(t-\tau)\dot{q}(\tau)\delta\tau \cong \begin{vmatrix} \dot{x}_r = A_r x_r + B_r \dot{q} \\ \mu = C_r x_r \end{vmatrix} \tag{9}$$

This process involves the identification of the state-space system with matrices A_r, B_r, and C_r, for each entry of the matrix K. The *SS_Fitting* toolbox developed and presented in this work derives these matrices, based on the WAMIT outputs. The toolbox is available at the NREL and Wave Energy Centre (WavEC) websites.[1]

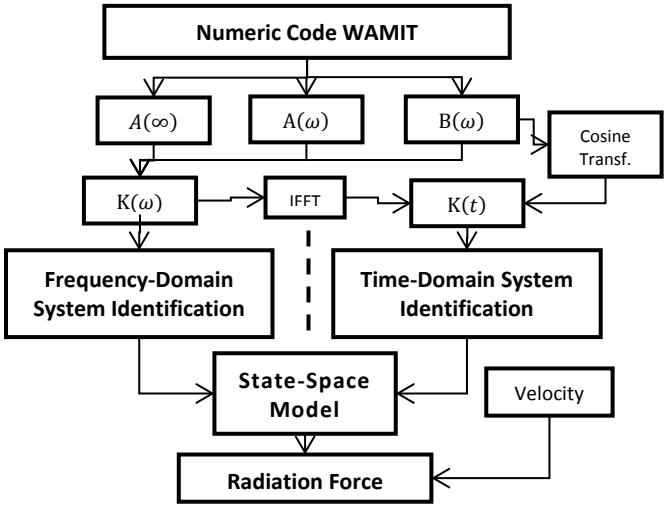

FIGURE 2. SCHEME OF THE RADIATION-FORCE CALCULATION USING FREQUENCY- OR TIME-DOMAIN IDENTIFICATION METHODS.

The retardation function in the frequency domain is simple to compute. Using Eq. (5) and the frequency response, it is possible to find the equivalent linear state-space model. This method is known as the *Frequency-Domain Identification*. However, using the inverse *Fourier Transform* method, or Eq. 8, it is possible to find the impulse-response function of the retardation function. In addition, it is possible to find the state-space model with the equivalent impulse response by using the *Time-Domain Identification*. These methods are summarized in Figure 2.

Because of these different approaches, several methods were proposed in the past literature to perform the system identification. For example, see [7], [8], [9], [10], [11], [12], [13], [14], [15], [16], and [17].

Using examples from the studies mentioned, we implemented four different methods within the *SS_Fitting* toolbox. As a result, the user can then choose which method to use and define in the input file (for more information, see [2]). The different methods are described in the following sections.

One of the advantages of the state-space model is the Markovian propriety, which guarantees that any future state of the system depends only on the present value of the system states. In other words, no past information needs to be stored, as in the case of the convolution method, because all of the memory effect is contained in the state vector x_r.

3.1. Constraints on Parametric Models

A parametric model (transfer function) can be fitted with the appropriate order for each entry of the retardation matrix:

$$\widetilde{K}_{ij}(s,\theta) = \frac{P(s,\theta)}{Q(s,\theta)} = \frac{p_m s^m + p_{m-1}s^{m-1} + \cdots + p_0}{s^n + q_{n-1}s^{n-1} + \cdots + q_0} \tag{10}$$

Where $\theta=[p_m,\ldots,\ p_0, q_{n-1}, \ldots, q_0]$ is a vector containing the different parameters of the numerator $P(s,\theta)$ and denominator $Q(s,\theta)$, $\widetilde{K}_{ij}$ is an entry of the retardation matrix of modes ij, $(i,j = 1,\ldots,6)$ and $s = j\omega$. The parametric models fitted to the retardation function should fulfill certain proprieties that are known *a priori*. These proprieties were derived using the hydrodynamic proprieties of the radiation potential in [18] and are summarized in Table 1.

3.1.1.Low-Frequency Asymptotic Value

The low-frequency asymptotic value is given by:

$$\lim_{\omega\to 0} K(\omega) = 0 \tag{11}$$

This statement is based on the principal that no structure can radiate waves at zero frequency. If the retardation function is approximated by Eq. (10), then the function has to have a zero at $s = 0$. This means that the parameter p_0 has to be zero.

3.1.2. High-Frequency Asymptotic Value

The high-frequency limit of the retardation function has to be zero:

$$\lim_{\omega\to\infty} K(\omega) = 0 \tag{12}$$

[1] www.wavec.org and http://wind.nrel.gov/

This limit can be proved by using Eq. (5). The damping limit has to be zero, because the excitation force for high frequency (short waves) also tends to zero, due to pressure cancellation on the body surface. The difference $A(\omega) - A_\infty$ will also drop to zero when $\omega \to \infty$.

To guarantee this propriety, the transfer function $K(j\omega)$ has to be strictly proper. That is, the degree of the denominator must be larger than the degree of the numerator ($\deg\{Q(s)\} > \deg\{P(s)\}$). This will guarantee that the denominator grows faster with ω than the numerator, and therefore the function will drop to zero when the frequency tends to infinite.

3.1.3. Initial Time Value

The impulse-response function of the retardation function must have an initial value other than zero. This can be proved by Eq. (13):

$$\lim_{t\to 0} K_{ij}(t) = \lim_{s\to\infty} sK_{ij}(s,\theta) = \lim_{s\to\infty} s\frac{P(s,\theta)}{Q(s,\theta)} = \frac{p_m s^{m+1}}{s^n} \qquad (13)$$

It is clear that, for the limit to be finite and different from zero, the relative order of the denominator and numerator must be one ($n = m + 1$).

Combined with the requirements of the first property described, it is easy to see that the minimum order function is second order, with the following format:

$$\widetilde{K}_{ij}^{min}(s) = \frac{p_1 s}{s^2 + q_1 s + q_0}, \qquad (14)$$

3.1.4. Final Time Value

The response of a stable system to an impulse should tend to zero when time tends to infinite. This propriety establishes the bounded-input bounded-output stability (BIBO) of the radiation system and is given by the limit:

$$\lim_{t\to\infty} K_{ij}(t) = \lim_{t\to\infty} {}^2/_\pi \int_0^\infty B(\omega)\cos(\omega t)\, d\omega = 0 \qquad (15)$$

Therefore, the poles of the transfer function $K_{ij}(s)$, given by the zeros of the denominator $Q(s)$, must have a negative real part.

3.1.5. Passivity

Passivity describes the propriety of systems that can store and dissipate energy, but not create it. When considering a floating body without external forces or incident waves, the *Cummins* equation can be written as:

$$M\ddot{q} \quad + C_{ij}^{hydrostatic} q = F^{radiation} \qquad (16)$$

The energy change of this system becomes:

$$E(T) - E(0) = \int_0^T F^{radiation}\dot{q} \quad dt \qquad (17)$$

Therefore, the convolution term of the radiation force has to be passive. See [18] and the related references for a more detailed derivation. For linear and time-invariant systems, passivity can be ensured if the retardation matrix is positive defined in the frequency domain:

$$\Re e\{\widetilde{K}_{ii}(s,\theta)\} = \Re e\left\{\frac{P_{ii}(s,\theta)}{Q_{ii}(s,\theta)}\right\} > 0 \qquad (18)$$

TABLE 1. PROPRIETIES OF RETARDATION FUNCTIONS

Propriety	Implications	Transfer Function
1. $\lim_{\omega\to 0} K(j\omega) = 0$	There are zeros at s=0	$p_0 = 0$
2. $\lim_{\omega\to\infty} K(j\omega) = 0$	Strictly proper	$\deg\{Q(s,\theta)\} > \deg\{P(s,\theta)\}$
3. $\lim_{t\to 0} K(t) \neq 0$	Relative degree 1	$\deg\{Q(s,\theta)\} - \deg\{P(s,\theta)\} = 1$
4. $\lim_{t\to\infty} K(t) = 0$	BIBO stability	$\Re e\{Q(s,\theta) = 0\} < 0$
5. The mapping $\dot{q} \to \mu$ is passive	$K(j\omega)$ is positive real	$\Re e\{\widetilde{K}_{ii}(s,\theta)\} = \Re e\left\{\frac{P_{ii}(s,\theta)}{Q_{ii}(s,\theta)}\right\} > 0$

3.2. Model Quality

Assessing the quality of the model can be done in several ways. As described earlier, the frequency-domain model is evaluated using the frequency response, while the time-domain models are evaluated by their impulse response. To evaluate these responses, the R^2 value is computed using:

$$R^2 = 1 - \frac{\sum_l (K_{ij} - \widetilde{K}_{ij})^2}{\sum_l (K_{ij} - \overline{K}_{ij})^2}, \qquad 0 \le R^2 \le 1 \qquad (19)$$

Where K_{ij} represents the reference retardation function, $\widetilde{K}_{ij}$ represents the parametric model, and $\overline{K}_{ij}$ represents the mean value of the reference retardation function. The summations are performed across all frequencies (for frequency response) or time (for impulse response). This is a measure of the amount of variability of the function that is captured by the model. The closer to one, the better is the quality of the fit.

3.3. Frequency Domain Identification

By providing the frequency response of the retardation function (computed with Eq. (5)), a transfer function can be fitted (as provided in Eq. (10)). However, the determination of the approximated models $\widetilde{K}_{ij}(s)$ poses an optimization problem following the least squares method, where the following equation is used to determine the transfer function parameters in the vector θ:

$$\theta = \arg\min_\theta \sum_s \left(K_{ij}(s) - \widetilde{K}_{ij}(s,\theta)\right)^2 \qquad (20)$$

This optimization problem can be solved by following the two methodologies presented in the following sections.

3.3.1. FREQ Method

This method is proposed by [19]. The least squares method is solved using the MatLab function *invfreqs* [20]. This function linearizes the optimization problem (20), using weight factors for the most important range of frequencies:

$$\theta = \arg\min_{\theta} \sum_{l} w_l \left(K_{ij}(s) - \widetilde{K}_{ij}(s,\theta) \right)^2 \quad (21)$$

Where w_l is the user-defined weighting vector with entries between zero and one for each frequency. The linearization method used by the MatLab function *invfreqs* is based on the Levy method [21].

The order of the transfer function is determined using an automatic routine. The problem is initialized using a second-order function, with the form:

$$\widetilde{K}_{ij}^{min}(s) = \frac{p_1 s + p_0}{s^2 + q_1 s + q_0}, \quad (22)$$

This equation is applied to guarantee the second propriety of Table 1. For each solution of the least squares method, the quality of the fit is evaluated using the parameter R^2, which is calculated using Eq. (19).

If the parameter R^2 is smaller than a given user-defined quality, the order of both the denominator and numerator of the transfer function is increased by one. Once the transfer function is found, it is easy to determine the equivalent state-space model using the MatLab function *tf2ss*. Refer to [19] and [22] for more detail.

Figure 3 presents an example of the application of this method to the pitch-surge cross term of the retardation matrix. As shown, the model $\widetilde{K}_{51}(s)$ does not fulfill the low-frequency limit. This model was derived for the spar buoy defined in Section 4.1, with a minimum R^2 of 0.97, which requires a third-order function.

3.3.2.FDI Method

The *SS_Fitting* toolbox developed with this work incorporates the frequency-domain identification toolbox (MSS FDI Toolbox) developed by [17]. The FDI toolbox is free and can be downloaded at www.marinecontrol.org.

This method is based on an approach that is similar to the one described in the previous section. However, three different methods are available to solve the optimization problem of Eq. (21), including:

- A linearized least squares minimization method
- A method that uses an iterative linear least squares problem
- A method that solves the nonlinear least squares problem, using a Gauss-Newton algorithm.

All of the methods use the MatLab function *invfreqs*. Based on the recommendations in [17], the iteratively linear least squares problem was chosen for this work because it provides the best computational time/accuracy relation. The FDI toolbox uses the following algorithm to take into account the proprieties of the retardation functions described earlier [23].

As noted earlier, the user defines the appropriate range of frequencies and the corresponding weight factors. The minimum order approximation is set to two. The parametric function is derived using:

$$\theta = \arg\min_{\theta} \sum_{l} \left| \frac{K_{ij}(s)}{s} - \frac{P'_{ij}(s,\theta)}{Q_{ij}(s,\theta)} \right|^2 \quad (23)$$

Where $P'_{ij}(s,\theta) = P_{ij}(s,\theta)/s$. The iterative method rewrites the previous equation in the linear form:

$$\theta_p = \arg\min_{\theta} \sum_{l} w_l s_{l,p} \left(Q_{ij}(s,\theta) K_{ij}(s) s^{-1} - P_{ij}(s,\theta) \right)^2 \quad (24)$$

where the coefficients are used from the previous iteration:

$$s_{l,p} = 1 \Big/ \left| Q_{ij}(s,\theta_{p-1}) \right|^2 \quad (25)$$

After a few iterations, the method converges ($\theta_{p-1} \sim \theta_p$) and the problem in Eq. (23) is obtained. If the return transfer function is not stable, the real part of the unstable roots of $Q_{ij}(s)$ is changed to a positive value, thereby ensuring the stability of the system. The final transfer function is reconstructed using:

$$\widetilde{K}_{ij} = \frac{s P_{ij}'(s,\theta)}{Q_{ij}(s,\theta)} \quad (26)$$

The added mass and damping are estimated based on the identified parametric approximation by:

$$\begin{aligned} \tilde{A}(\omega) &= Im\{\widetilde{K}_{ij}(\omega)\} + A(\infty) \\ \tilde{B}(\omega) &= \Re e\{\widetilde{K}_{ij}(\omega)\} \end{aligned} \quad (27)$$

and compared with the $A(\omega)$ and $B(\omega)$ provided by the hydrodynamic code. The quality of the fit is assessed using the parameter R^2, via Eq. (19) for the added mass and damping coefficients. If the fitting is not satisfactory, the order of the approximation is increased by one and the process starts over with Eq. (23). Finally, the toolbox checks if the solution is passive $\left(\Re e\{\widetilde{K}_{ii}(s,\theta)\} > 0\right)$.

As the transfer function is fitted to the primitive of the retardation function, which is accomplished by dividing by s in the frequency domain, we ensure that the first propriety of Table 1 is fulfilled, as the value of p_0 in Eq. (26) is going to be zero. The second and third proprieties are fulfilled, thereby confirming that the relative order of the functions is always one. This method ensures that most of the proprieties in Table 1 are met, and that this *a priori* knowledge is incorporated in the fitted functions. As a result, analysts can achieve a more accurate transfer function with a lower order. Using the transfer

functions, it is once again easy to obtain the state-space model (via tf2ss.m).
Figure 3 presents the approximation obtained with this method. As shown, the low-frequency limit is fulfilled and the required quality is achieved using only a second-order function.

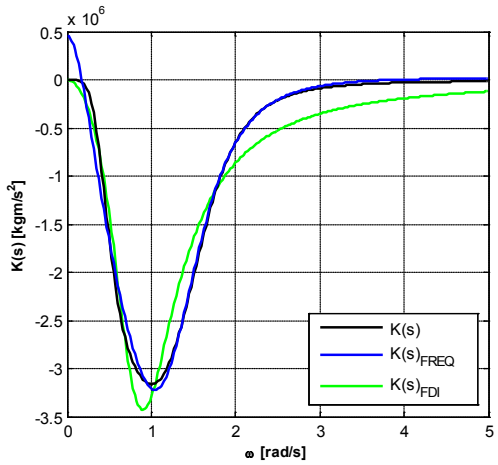

FIGURE 3. EXAMPLE OF THE PITCH-SURGE ENTRY OF THE RETARDATION MATRIX, USING THE FREQ AND FDI METHODS.

3.4. Time-Domain Identification

The identification of the state-space models can be based on the impulse-response function of the retardation matrix, as shown in Figure 2. The conversion to the time domain adds an additional error avoided in the frequency domain methods. However, this error can be minimized, depending on the method to convert $K_{ij}(\omega)$ into the time domain. The time-domain retardation function can be computed by using:

$$K_{ij}(t) = IFFT\left(K_{ij}(\omega)\right) \tag{28}$$

However, this method is limited by the Nyquist frequency limit. Because of the limited range of frequency usually used in the numerical codes, the discretization of $K_{ij}(t)$ will be evenly spaced and computed from zero to high values of t. This may lead to a poor description of the functions for low values of t, where the impulse response $K_{ij}(t)$ changes significantly.
An alternative method to compute the impulse-response function of the retardation matrix is to use the cosine transformation described in Eq. (8). This transformation was implemented using a trapezoidal integration method, as described in [13]:

$$K_{ij}(t) = \frac{\Delta\omega}{\pi}\sum_{k=1}^{k_{max}-1} 2B_{ij}(k\Delta\omega)\cos(k\Delta\omega t)\ldots \\ \ldots + \frac{\Delta\omega}{\pi}\left(B_{ij}(0) + B_{ij}(k_{max})\cos(k_{max}\Delta\omega t)\right) \tag{29}$$

Where k_{max} is the number of entries of the frequency vector computed by the numerical code. The step size used is determined by the length of the frequency vector, which is equally spaced using 256 points (e.g., for $k_{max}\Delta\omega = 5rad/s$, $\Delta\omega \cong 0.02\,rad/s$). The upper limit is taken to be $T = 100s$, and the time step used is $\Delta t = 0.1s$.
This last method was used to compute the impulse-response function necessary to implement the following time-domain methods.

3.4.1. Least Squares Method

The least squares method was used to determine the realization of the retardation function, and was implemented in [19].
This method is based on the MatLab function *prony*, which uses the *z-transform* to find the corresponding rational system function. The function returns the coefficients of numerator $b[k]$ and denominator $a[l]$ of the discrete rational system:

$$H(z) = \frac{\sum_{k=0}^{q} b[k]z^{-k}}{1 + \sum_{l=0}^{p} a[l]z^{-l}} \tag{30}$$

From the transfer functions, it is once again easy to obtain the state-space model (via *tf2ss.m*).
The discrete transfer function needs to be converted to the continuous time domain, using the MatLab function *d2c*, with the Tustin method. However, for complex, high-order retardation functions, this method does not ensure the stability of the resulting state-space model.
The order of the transfer function is determined by assessing the quality of the fit using the R^2 value, as described in Section 3.2.
Figure 4 shows the impulse-response function obtained with Eq. (29) $\left(\mathrm{K(t)}\right)$ and the estimated model $\left(\widetilde{\mathrm{K}}\mathrm{(t)}\right)$. The required R^2 for this case was 0.97, and this method derived a fourth-order model.

3.4.2.Realization Theory

Once the impulse-response function is obtained by (29), an identification scheme based on the Hankel Singular Value Decomposition (SVD) is applied. This method was proposed by [24] and is available in the MatLab function *imp2ss*. For a detailed description of the SVD method, consult [24].

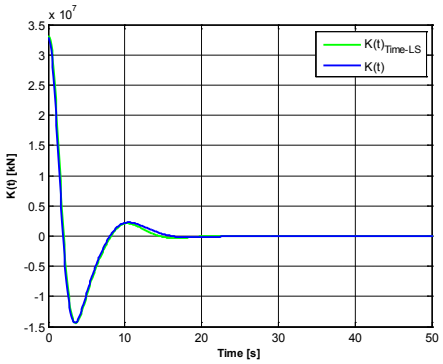

FIGURE 4. EXAMPLE OF THE PITCH-SURGE ENTRY OF THE IMPULSE RESPONSE MATRIX, USING THE TIME LEAST SQUARES METHOD.

The function outputs the matrixes of the equivalent state-space system, $\overline{A_r}$, $\overline{B_r}$, $\overline{C_r}$, and $\overline{D_r}$, which need to be scaled according to the time step used in $K\ \ (t)$:

$$A_r = \overline{A_r}\,, \qquad B_r = \overline{B_r}\,, \qquad C_r = \overline{C_r}\Delta t\ \ D_r = \overline{D_r}.0 = 0 \qquad (31)$$

The matrix D_r is forced to be zero to keep the causality of the system. Despite the reduction option that is built into the *imp2ss* function, this does not prove to be a satisfactory way to control the accuracy and order of the fitted model. The function produces very accurate models ($R^2 > 0.99$), but uses a very high order ($i > 200$). However, the computations of the Hankel singular values revealed that only a small number of states have a significant value (e.g., Figure 5).

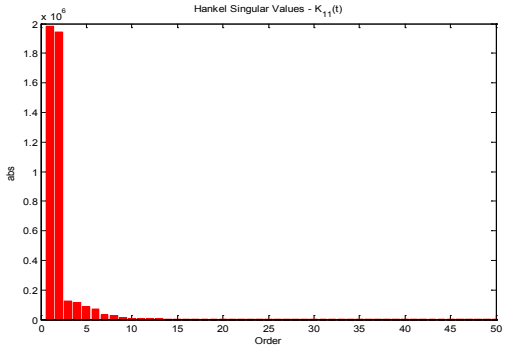

FIGURE 5. HANKEL SINGULAR VALUES OF THE IMPULSE-RESPONSE FUNCTION SURGE-SURGE FOR THE OFFSHORE CODE COMPARISON COLLABORATION (OC3)-HYWIND SPAR BUOY.

Figure 5 clearly shows that the first two singular values have an absolute value that is much higher than all of the others. In fact, this function can be approximated with a second-order system with $R^2 > 0.98$.

To obtain a low-order model, we reduced the number of states by using the MatLab function *balmr*. This function can apply two methods: 1) the manual method, where the user chooses the number of states to keep, based on the Hankel Singular Values plot, and 2) the automated method, which is implemented using the goodness of the fit R^2 calculated with Eq. (19) for the impulse-response function. This step reduces the number of states to a second-order function, and then increases the order of the system until the user-defined goodness is achieved.

4. MODEL COMPARISON

4.1. Reference Case

To compare the quality of the fit of the models obtained from the four different methods, we considered two platform designs. The first was the spar buoy used in the Offshore Code Comparison Collaboration (OC3) studies, named *OC3-Hywind* [25], in which the design is based on the *Hywind* prototype and consists of a ballast-stabilized buoy with 120 m of draft. Its cylindrical shape minimizes the wave radiation, thereby providing very simple radiation impulse-response functions.

The Offshore Code Comparison Collaboration Continuation (OC4) semisubmersible platform was the other design used in this study [26]. It consists of a triangular-shaped semisubmersible platform with three main offset columns and the turbine placed on a fourth central column. The more complex shape of the design provides higher-order impulse-response functions, as shown in Figure 7.

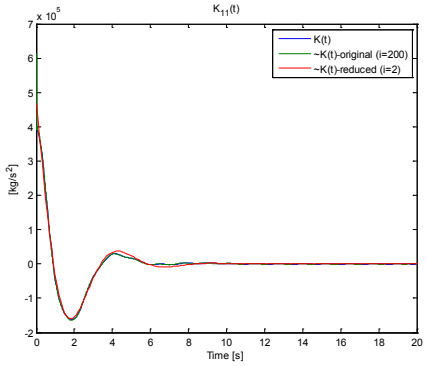

FIGURE 6. EXAMPLE OF THE PITCH-SURGE ENTRY OF THE IMPULSE RESPONSE, USING THE REALIZATION THEORY METHOD.

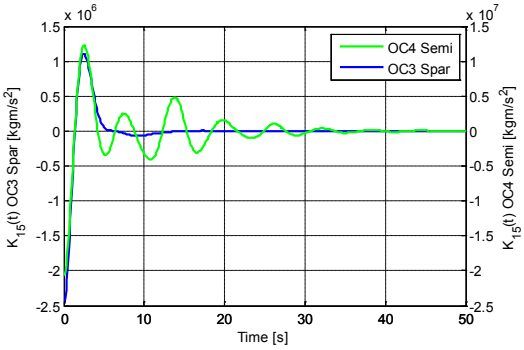

FIGURE 7. IMPULSE-RESPONSE FUNCTION K_{15}, FOR THE OC3 SPAR AND OC4 SEMISUBMERSIBLE PLATFORMS.

To compare the results of the state-space model with the currently implemented numerical convolution method in FAST, 1-hr long simulations were run using stochastic waves with 6-m significant height and a peak period of 10 s. We also performed a sensitivity analysis of the system response using different wave periods (a period range between 2 and 17 s, according to Table 2). The sensitivity analysis results are presented in Section 5.

TABLE 2. REFERENCE SEA STATES

Sea State	***1***	***2***	***3***	***4***	***5***	***6***	***7***	***8***
$H_s\ [m]$	0.09	0.67	1.40	2.44	3.66	5.49	9.14	15.24
$T_p\ [s]$	2.0	4.8	6.5	8.1	9.7	11.3	13.6	17.0

4.2. Model Quality

For the simple case of the spar buoy, different methods were run using a minimum required R^2 value of 0.97. Figures 8 and 9 show the quality of the fit for the different methods compared to the number of states that were needed to represent them. This comparison was done based on the reference retardation function obtained from the WAMIT outputs, using Eq. (5) for

the frequency response and Eq. (8) for the time response. In figures 8 and 9, each dot represents the quality and order of the transfer function corresponding to each significant entry of the retardation matrix. The total number is the sum of the number of states used to describe each entry of K.

The FDI method provided the lowest number of states than the other methods. However, the R^2 was slightly lower than the rest, sometimes even lower than 0.97, as the FDI method used the added mass and damping coefficients as the reference, and not the retardation function directly.

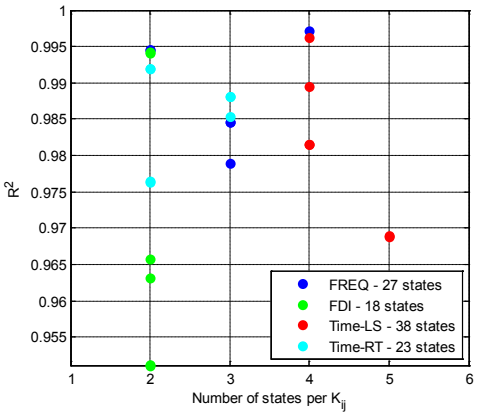

FIGURE 8. QUALITY OF THE FREQUENCY RESPONSE OF THE DIFFERENT METHODS, FOR THE OC3-HYWIND SPAR BUOY AND A REQUIRED R^2 VALUE OF 0.97.

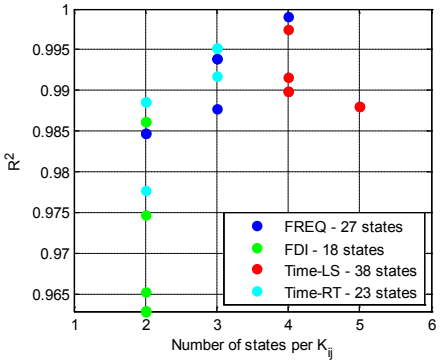

FIGURE 9. QUALITY OF THE IMPULSE RESPONSE OF THE DIFFERENT METHODS FOR THE OC3-HYWIND SPAR BUOY AND A REQUIRED R^2 VALUE OF 0.97.

The realization method (Time–RT) also provided a low number of states with a good model quality. Despite being a time-domain method, it also appeared to fit the frequency response with a good model quality.

In addition, the frequency method (FREQ) provided a good fit; both in the frequency and impulse response. However, it required a significantly higher number of states to achieve the same quality.

Finally, the time-domain least squares method (Time-LS) required the highest number of states, and it did not guarantee a good fit of the frequency response.

Figure 10 shows the response of the surge-pitch term of the retardation matrix. As presented earlier, the system's frequency and impulse responses were accurately fitted by all of the methods (first and second graphs in Figure 10). However, these figures show that, despite the absolute value of frequency response being well-approximated, the low-frequency limit of the added mass and damping (third and fourth graphs in Figure 10) presents significant differences. The FDI method provides an accurate solution for this low-frequency limit, as it incorporates this constraint *a priori*. The time-domain least squares method also fits this limit, but uses a much higher number of states. The implication of these differences is presented in more detail in Section 5.1.

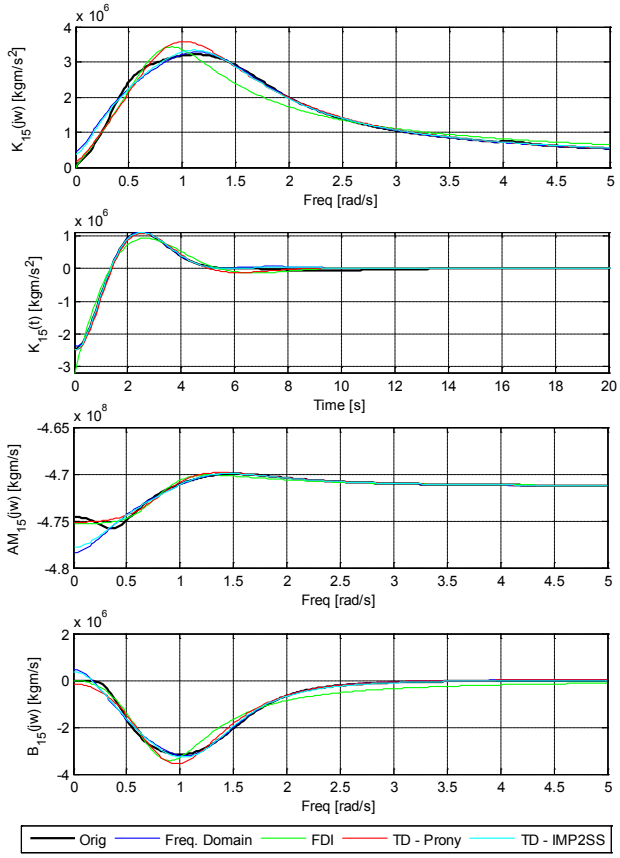

FIGURE 10. MODEL COMPARISON FOR THE OC3-HYWIND SPAR BUOY, USING THE SURGE-PITCH TERM OF THE RETARDATION MATRIX, FROM TOP TO BOTTOM: FREQUENCY RESPONSE, IMPULSE RESPONSE, ADDED MASS, AND DAMPING COEFFICIENT.

4.3. Number of States Versus R^2

To guarantee a low simulation time and application to controls design, the number of states must be as low as possible. The different methods used provide very different model orders for the same requested R^2 value. Figure 11 shows the number of states of the models obtained with the different methods, both for the OC3 spar and the OC4 semisubmersible, for different values of R^2.

As shown, it is possible to fit a high-quality model with a low number of states for the spar buoy case, because of its simple geometry. In the opposite case, the OC4 semisubmersible required much higher-order models. When comparing the different methods, it is clear that the FDI and Time-RT methods provided the lowest-order models. The Time-LS method

required a high number of states, and was unable to provide a stable system for the case of the OC4 semisubmersible for R^2 higher than 0.85. The FREQ method was able to provide a stable system, but with a very high number of states, especially for the OC4 semisubmersible.

5. TIME-DOMAIN MODEL

This section compares the forces calculated using the state-space module (*SS_Radiation*), with the forces obtained by the numerical convolution method implemented in FAST's HydroDyn module. The *SS_Radiation* module was integrated within the HydroDyn code written in the new FAST modularization framework. However, the new HydroDyn module was not integrated within FAST at the time of these tests. Therefore, FAST was run separately for the desired load case, and outputting the radiation forces and moments and the platform velocities. The platform velocities were used as an input in the HydroDyn and state-space modules, using the models derived from the different methods presented earlier. The new *SS_Radiation* module was compared to the convolution method existing within HydroDyn.

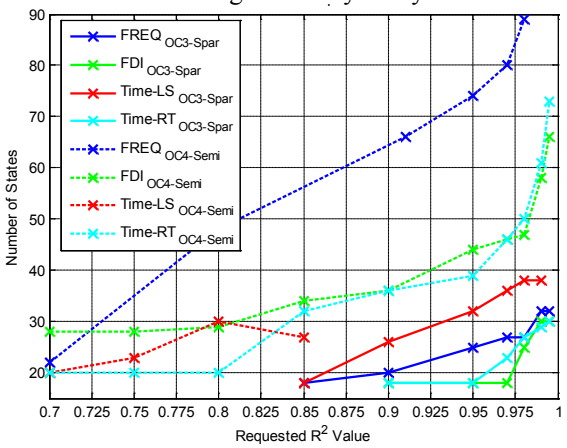

FIGURE 11. MODEL ORDER FOR DIFFERENT R^2 VALUES.

This uncoupled approach of testing the *SS_Radiation* module represents the best-case scenario, as the error in the radiation forces did not build up along the simulation because of drift in the platform velocities. However, as the radiation force is significantly smaller than other hydrodynamic forces in play (for the platforms studied), the changes in the platform motions caused by the accumulated error should not affect the results significantly.

5.1. Accuracy of State-Space Models

Figure 12 presents the time evolution of the radiation forces in surge and pitch for the different state-space models compared to the results from HydroDyn (using a memory time of 60 s). The models were derived using $R^2 = 0.97$ and provided results that were similar to the convolution method.

The bigger differences occurred for the least energetic degrees of freedom—namely sway and roll (because the incoming waves were orientated with the surge axis (not shown)). The time-domain least squares method provided the worst agreement with the forces predicted by the convolution method, probably due to low stability margins.

Figure 13 shows the agreement between the convolution method and the state-space method (R^2_{conv}), for different fitting methods and requested R^2 values. For the case of the spar buoy (solid lines), most of the methods agreed with the convolution method, except for the time-domain least squares method. Despite providing a good fit with the impulse response, the resulting state-space models had low stability margins, thereby agreeing poorly with the convolution method.

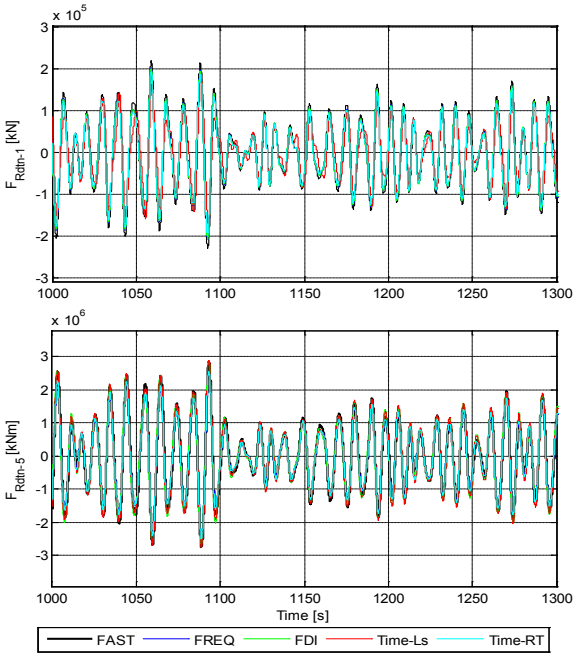

FIGURE 12. RADIATION FORCES FOR THE OC3-HYWIND SPAR BUOY, USING THE NUMERICAL CONVOLUTION AND DIFFERENT STATE-SPACE MODELS EMPLOYING $R^2 = 0.97$.

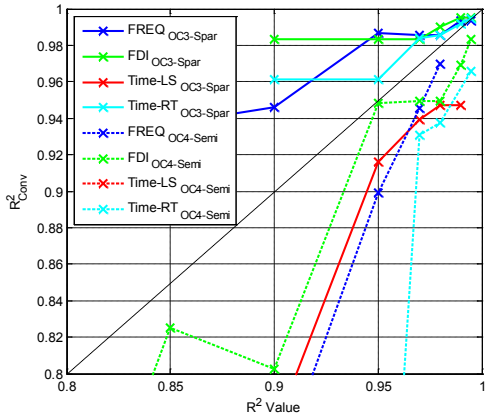

FIGURE 13. QUALITY OF THE FIT OF THE STATE-SPACE MODELS AGAINST THE CONVOLUTION METHOD (R^2_{conv}) VERSUS THE REQUESTED R^2 VALUE FOR THE DIFFERENT MODELS.

For the OC4 semisubmersible platform case (dashed lines), the methods provided a slightly worse agreement than in the spar case. Instead, the frequency-domain methods provided a better prediction of the radiation forces than the realization theory method. However, the FREQ method required a significantly

larger number of states, as shown in Figure 3. The FDI method provided a low number of states while agreeing with the convolution method. As discussed in Section 4.2, this result was achieved by including the constraints presented in Section 3.1 *a priori*.

Figure 14 presents a sensitivity analysis of the agreement between the surge force obtained with the convolution and state-space methods for the different sea states presented in Table 2.

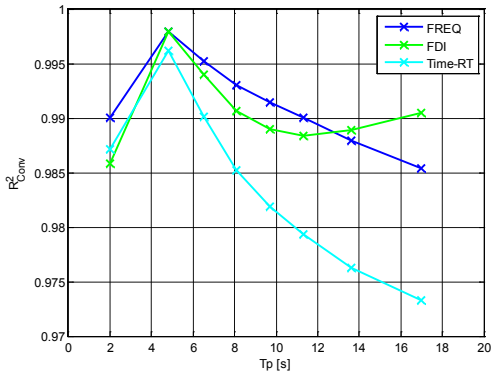

FIGURE 14. AGREEMENT BETWEEN THE CONVOLUTION METHOD AND THE STATE-SPACE MODELS FOR THE SURGE-SURGE FORCE (USING $R^2 = 0.97$) FOR DIFFERENT SEA STATES.

As shown in Figure 14, all of the methods provided a poor response for high-frequency sea states, ($Tp < 4\ s$). This response occurs because the models were derived with a weight vector w_l (see Eq. (21)) of 1, between 0 and 2.5 rad/s (and zero for the other frequencies), as this range comprises the most common wave-frequency range. It can also be seen that, for the low-frequency limit ($Tp > 10\ s$), the accuracy of the methods is reduced. This is in accordance with the findings described in Section 4.2. The FDI method is the only method that guarantees good accuracy for the low-frequency, high-energetic waves, as it forces this constraint into the derived model.

As shown earlier, the state-space models provided an accurate method to predict the radiation forces, using R^2 values larger than 0.97. However, when considering the other hydrodynamic forces, namely hydrostatic, diffraction, and viscous forces, the comparison of the total hydrodynamic forces results in R^2 very close to 1, even for models derived with R^2 values of 0.8. This shows the order of magnitude of the radiation forces when compared with other hydrodynamic forces. Because of this effect, the authors of [23] suggest using a smaller-order model to reduce the chances of a significant loss of accuracy in the overall result. Although this approach may not be important for a single wind turbine, it might be useful for reducing the model order and gaining computational speed of multiple floating wind turbines.

5.2. Computational Time of the *SS_Radiation* Module

Figure 15 shows the time ratio, defined as:

$$T_{ratio} = {}^{T_{sim}}/_{T_{CPU}}, \qquad (32)$$

of the *SS_Radiation* module. As shown, the ratio decreases (as expected) with the order of the model (number of states), and it seems to be independent of the model used. Despite the significant increase in computational time, the time ratio remains above 1000 in all cases (as the model order increases).

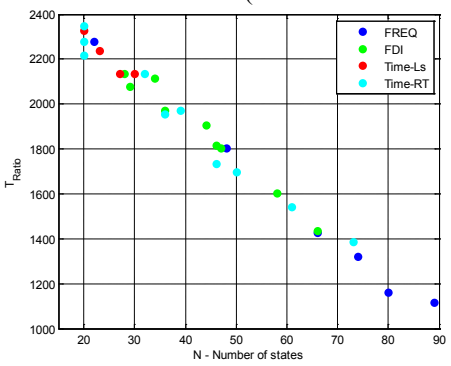

FIGURE 15. SIMULATION TIME RATIO OF THE STATE-SPACE MODULE, USING DIFFERENT NUMBERS OF STATES.

5.3. Convolution Versus State-Space

During this part of the study, the new version of the HydroDyn code was used with the convolution and state-space methods to compute the wave-radiation loads. As discussed earlier, the platform velocities obtained from FAST were fed to the modules.

Using this new module, a sensitivity analysis was performed to check the accuracy and computational time of the convolution method, thereby changing the memory time (as shown in Eq. (4)). The results are presented in Figure 16. The memory time varied from 1 to 210 s, and the highest value was taken as a reference to assess the quality of the fit.

For comparison purposes, the results obtained from the state-space module using the FDI method are presented in the figure, using the number of states as a reference.

The shape and impulse-response functions, discussed in Section 4.1, had a significant influence on the accuracy of the methods. The convolution method required 10 s of memory for the spar and 20 s for the semisubmersible to achieve good accuracy. A value closer to one was achieved for a memory time of 60 s. As shown in Figure 7, the impulse response is close to zero after 50 s. The results obtained for the state-space methods are in accordance with the ones discussed earlier.

Figure 17 compares the computational time and accuracy of both the convolution and state-space methods. The convolution method achieves high accuracy when compared to the state-space method, at the cost of a higher computational time. Using a memory time of 60 s, the time ratio of the convolution method is around 200 for both platforms. For the state-space method, there is a large variance of the computational time, especially in the spar case, but in general, much higher time ratios (>800) can be achieved. This improvement represents a time reduction of 75% in the computation of the wave-radiation forces.

When using a complex wind turbine model with all of the available degrees of freedom and control system enabled, and under turbulent wind and stochastic wave conditions, the wave radiation forces in FAST still account for 40% of the computational time when using 60 s of memory. Therefore, a reduction of up to 30% of FAST computational time can be expected when using the state-space method.

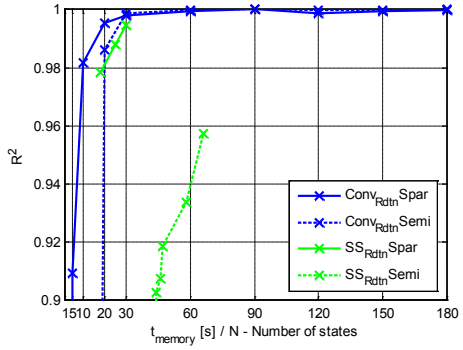

FIGURE 16. ACCURACY OF THE CONVOLUTION AND STATE-SPACE METHODS.

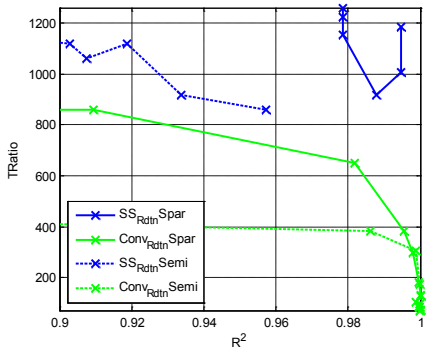

FIGURE 17. COMPUTATIONAL TIME VERSUS ACCURACY OF THE CONVOLUTION AND STATE-SPACE METHODS FOR DIFFERENT PLATFORMS.

6. CONCLUSIONS

In this paper, we presented four methods to fit a state-space model of the wave-radiation forces. These methods were developed and included in the new MatLab toolbox *SS_Fitting* and their required model order and accuracy were compared to the WAMIT outputs. The frequency-domain method based on the MatLab frequency-domain identification (FDI) toolbox and the time-domain method based on the realization method proved to offer the best quality fit with the smallest number of states.

The MatLab toolbox was designed to provide the state-space matrices needed by the new radiation module in FAST, *SS_Radiation*. However, the accuracy of this method decreases for platforms that have complex shapes. As a result, a R^2 value of at least 0.97 should be required when fitting the state-space models. Compared to the convolution method, the new module is 75% faster, which can be translated into a 30% reduction of the total FAST computational time. However, the accuracy and computational time should be re-evaluated when a coupled version of the new HydroDyn and FAST becomes available.

7. ACKNOWLEDGMENTS

The first author would like to acknowledge the project funding provided by the Fulbright Commission, under the Fulbright Research Grant program. The third author performed this work at the National Renewable Energy Laboratory in support of the U.S. Department of Energy, under contract number DE-AC36-08GO28308 and under a project funded through topic area 1.1 of the Funding Opportunity Announcement (FOA) number DE-FOA-0000415.

8. REFERENCES

[1] NREL, "NWTC Computer-Aided Engineering Tools (FAST by Jason Jonkman, Ph.D.)," 02 11 2012. [Online]. Available: http://wind.nrel.gov/designcodes/simulators/fast/. [Accessed 12 11 2012].

[2] T. Duarte, "SS_Fitting User Manual," NREL, Golden, CO, 2012.

[3] J. Jonkman, "The New Modularization Framework for the FAST Wind Turbine CAE Tool," NREL, Golden,CO, 2013.

[4] W. Cummins, "The impulse response function and ship motion," David Taylor Model Basin-DTNSRDC, 1962.

[5] WAMIT, "WAMIT User Manual (V7)," 2012. [Online]. Available: http://www.wamit.com.

[6] T. Ogilvie, "Recent progress towards the understanding and prediction of ship motions," in *6th Symposium on Naval Hydrodynamics*, 1964.

[7] E. Jefferys, D. Broome and M. A. Patel, "A transfer function method of modelling systems with frequency dependant coefficients," *Journal of Guidance Control and Dynamics,* vol. 7(4), p. 490–494, 1984.

[8] E. Jefferys and K. Goheen, "Time domain models from frequency domain descriptions: Application to marine structures," *International Journal of Offshore and Polar Engineering,* p. 2:191–197, 1992.

[9] Z. Yu and J. Falnes, "Spate-space modelling of a vertical cylinder in heave," *Applied Ocean Research,* pp. 17:265-275, 1995.

[10] Z. Yu and J. Falnes, "State-space modelling of dynamic systems in ocean engineering," *Journal of hydrodynamics,* pp. 1-17, 1998.

[11] K. Holappa and J. Falzarano, "Application of extended state space to nonlinear ship rolling," *Ocean Engineering,* vol. 26, pp. 227-240, 1999.

[12] A. Hjulstad, E. Kristansen and O. Egeland, "State-space representation of frequency-dependant hydrodynamic coefficients," in *Proc. IFAC Conference on Control Applications in Marine Systems*, 2004.

[13] E. Kristansen and O. Egeland, "Frequency dependent added mass in models for controller design for wave motion ship damping," Girona, Spain, 2003.

[14] E. Kristiansen, A. Hjuslstad and O. and Egeland, "State-space representation of radiation forces in time-domain vessel models," *Ocean Engineering,* vol. 32, p. 2195–2216, 2005.

[15] M. Jordan and R. Beltran-Aguedo, "Optimal identification of potential-radiation hydrodynamics of moored floating stuctures," *Ocean Engineering,* vol. 31, p. 1859–1914, 2004.

[16] A. McCabe, A. Bradshaw and M. Widden, "A time-domain model of a floating body usign transforms," in *Proc. of 6th European Wave and Tidal Energy Conference*, University of Strathclyde, Glasgow, U.K., 2005.

[17] T. Perez and T. Fossen, "A matlab toolbox for parametric identification of radiation-force models of ships and offshore structures," *Modeling Identification and Control,* vol. 30(1), pp. 1-15, 2009.

[18] T. Perez and T. Fossen, "Time- vs. Frequency-domain Identification of Parametric Radiation Force models for Marine Structures at Zero Speed," *Modeling, Identification and Control,* vol. 29, pp. 1-19, 2008.

[19] M. Alves, M. Vicente, A. Sarmento and M. Guerinel, "Implementation and verification of a time domain model to simulate the dynamics of OWCs," Southampton, 2011.

[20] Mathworks, "MATLAB User Manual".

[21] E. Levy, "Complex Curve Fitting," *IRE Trans. Autom. Control,* Vols. AC-4, pp. 37-43, 1959.

[22] M. Alves, "Numerical Simulation of the dynamics of poit absorber wave energy converters using frequency and time domain approaches," Technical University of Lisbon, PhD Thesis, Lisboa, 2012.

[23] T. Perez and T. Fossen, "Pratical apsects of frequency-domain identification of dynamic models of marine structures from hydrodynamic data," *Ocean Engineering,* vol. 38, pp. 426-435, 2011.

[24] S. Y. Kung, "A new identification and model reduction algorithm via singular value decomposition," in *Twelfth Asimolar Conf. on Circuits, Systems and Computers*, 1978.

[25] J. Jonkman, "Definition of the Floating System for Phase IV of OC3," NREL, Golden, Colorado, 2010.

[26] A. Robertson, J. Jonkman, M. Masciola, H. Song, A. Goupee, A. Coulling and C. Luan, "Definition of the Semisubmersible Floating System for Phase II of OC4," NREL, Golden, CO, 2012.